Since January 2020 Elsevier has created a COVID-19 resource centre with free information in English and Mandarin on the novel coronavirus COVID-19. The COVID-19 resource centre is hosted on Elsevier Connect, the company's public news and information website.

International Journal of Pharmaceutics 603 (2021) 120701

Contents lists available at ScienceDirect

International Journal of Pharmaceutics

journal homepage: www.elsevier.com/locate/ijpharm

Niclosamide inhalation powder made by thin-film freezing: Multi-dose tolerability and exposure in rats and pharmacokinetics in hamsters

Miguel O. Jara [a], Zachary N. Warnken [a,*], Sawittree Sahakijpijarn [a], Chaeho Moon [a], Esther Y. Maier [b], Dale J. Christensen [c], John J. Koleng [c], Jay I. Peters [d], Sarah D. Hackman Maier [e], Robert O. Williams III [a,*]

[a] Molecular Pharmaceutics and Drug Delivery Division, College of Pharmacy, The University of Texas at Austin, 2409 University Avenue, Austin, TX 78712, USA
[b] Drug Dynamics Institute, College of Pharmacy, The University of Texas at Austin, Austin, TX 78712, USA
[c] TFF Pharmaceuticals, Inc., Austin, TX 78746, USA
[d] UT- Health San Antonio Department of Medicine, Division of Pulmonary/Critical Care Medicine, San Antonio, TX 78229, USA
[e] UT- Health San Antonio Department of Pathology, San Antonio, TX 78229, USA

ARTICLE INFO

Keywords:
Pulmonary administration
Thin Film Freezing
Niclosamide
Lung pharmacokinetics
Dry powder inhaler
SARS-CoV-2

ABSTRACT

In this work, we have developed and tested a dry powder form of niclosamide made by thin-film freezing (TFF) and administered it by inhalation to rats and hamsters to gather data about its toxicology and pharmacokinetics. Niclosamide, a poorly water-soluble drug, is an interesting drug candidate because it was approved over 60 years ago for use as an anthelmintic medication, but recent studies demonstrated its potential as a broad-spectrum antiviral with pharmacological effect against SARS-CoV-2 infection. TFF was used to develop a niclosamide inhalation powder composition that exhibited acceptable aerosol performance with a fine particle fraction (FPF) of 86.0% and a mass median aerodynamic diameter (MMAD) and geometric standard deviation (GSD) of 1.11 μm and 2.84, respectively. This formulation not only proved to be safe after an acute three-day, multi-dose tolerability and exposure study in rats as evidenced by histopathology analysis, and also was able to achieve lung concentrations above the required IC_{90} levels for at least 24 h after a single administration in a Syrian hamster model. To conclude, we successfully developed a niclosamide dry powder inhalation that overcomes niclosamide's limitation of poor oral bioavailability by targeting the drug directly to the primary site of infection, the lungs.

1. Introduction

The Coronavirus Disease 2019 (COVID-19) is a pandemic caused by the coronavirus (CoV), also known as Severe Acute Respiratory Syndrome Coronavirus 2 (SARS-CoV-2). SARS-CoV-2 is related to other CoVs that have caused other pandemics, including Severe Acute Respiratory Syndrome (SARS) and the Middle East Respiratory Syndrome (MERS) in 2002–2003 and 2012, respectively (Miller et al., 2020; Wu et al., 2020). Currently, the COVID-19 pandemic has unfortunately killed more people than either of the other before-mentioned pandemics combined (Gurwitz, 2020; Miller et al., 2020; Xue et al., 2020).

In 2004, Wu *et al.* reported that the FDA-approved drug niclosamide inhibits the viral replication of SARS-CoV (Wu et al., 2004). More recently, in 2019, niclosamide was shown to inhibit the viral replication of MERS-CoV by more than a 1000-fold by interfering in pathways related to the proteasome and autophagy mechanisms (Gassen et al., 2019; Xu et al., 2020). Now, in 2020, during the COVID-19 pandemic, niclosamide has shown very promising effectiveness against the viral replication of SARS-CoV-2 with a reported IC_{50} of 0.28 μM (~91.56 ng/mL) by similar reported mechanisms of action as that reported for SARS-CoV, and the mechanisms of anti-viral activity may include potentially direct intermolecular interactions between the drug and SARS-CoV-2 proteins (Jeon et al., 2020; Pindiprolu and Pindiprolu, 2020; Romani et al., 2020; Xu et al., 2020). Based on the data reported by Jeon et al., Arshad et al. (2020) estimated an IC_{90} of 153.7 ng/mL for niclosamide (Arshad et al., 2020). This evidence supports niclosamide as a candidate for repurposing as an antiviral for the current pandemic.

Unfortunately, niclosamide is a poorly water-soluble molecule with limited oral bioavailability, thus limiting its ability to be repurposed for other clinical indications. The clearest example of this limitation is

* Corresponding authors.
E-mail addresses: zwarnken@utexas.edu (Z.N. Warnken), bill.williams@austin.utexas.edu (R.O. Williams III).

https://doi.org/10.1016/j.ijpharm.2021.120701
Received 3 March 2021; Received in revised form 5 May 2021; Accepted 8 May 2021
Available online 12 May 2021

clinical trial NCT02532114 that was terminated prematurely due to the low and variable bioavailability of niclosamide, reportedly only reaching C_{max} values between 35.7 and 182 ng/mL when administered orally at 500 mg three-times-daily (Schweizer et al., 2018). However, SARS-CoV-2 mainly affects the pulmonary airways; the virus has a tropism towards alveolar macrophages and pneumocytes (type I and II) (Chu et al., 2020). Here the virus leads to breathing difficulties, acute respiratory distress syndrome, pneumonia, among other complications (Damiani et al., 2021; Guan et al., 2020). A way to overcome niclosamide's severe bioavailability limitation and deliver the drug in efficient concentrations to the lungs is by the development of niclosamide as an inhaled product. Niclosamide has been reported to be safe for inhalation after 24 h of administration (Costabile et al., 2015). However, to the best of our knowledge, a pharmacokinetic evaluation of inhaled niclosamide has not previously been reported.

Thin-film freezing (TFF) is a technology used for particle engineering, usually aiming to develop powders for inhalation for use with dry powder inhalers (DPI). The TFF-processed powders generally are low-density, brittle, and porous matrices with excellent aerosol performance (Beinborn et al., 2012). The TFF technology generates these powders by fast supercooling of drug-carrier solutions (sometimes suspensions) (Moon et al., 2019). The frozen material then is lyophilized to remove the employed solvents (e.g., acetonitrile, 1,4 dioxane, *tert*-butanol or water). TFF technology has proven to be useful in generating powders for delivery by DPI, and currently, there are two formulations in phase I clinical trials (i.e., voriconazole and tacrolimus) using this established technology (AboulFotouh et al., 2020; Almansour et al., 2020; Mattes, n.d., Sagan, n.d.). For these reasons, the development of an inhaled niclosamide powder by TFF is hypothesized to offer a new therapeutic option and route of administration in the fight against COVID-19.

In this work, we aim to develop a formulation to reach the lungs and sustain niclosamide concentrations, which is difficult to achieve by other routes of administration due to niclosamide's poor-water solubility and high first-pass metabolism (Barbosa et al., 2019; Lu et al., 2016). For this purpose, the niclosamide inhalation powder requires aerodynamic diameters between 1 and 5 μm, necessary for lung delivery where it can exert its pharmacological effect (Mönckedieck et al., 2017).

The goals of the research are summarized as follows: (1) develop a dry powder of niclosamide for inhalation by TFF manufacturing as a potential therapeutic for COVID-19; (2) test its *in vitro* aerodynamic properties; 3) characterize its solid-state properties; and (4) evaluate its lung toxicity using the rat model and its pharmacokinetics using the Syrian golden hamster model.

2. Materials and methods

2.1. Materials

Niclosamide was purchased from Shenzhen Nexconn Pharmatechs LTD. (Shenzhen, China). Tert-butanol (TBA), acetone, acetonitrile, leucine, polysorbate 20, trifluoracetic acid were acquired from Fisher Scientific (Pittsburgh, PA, USA). Pearlitol® PF-mannitol was purchased from Roquette America (Keokuk, IA, USA).

2.2. Preparation of thin film freezing (TFF) composition

In the preparation of the solutions for TFF manufacturing, niclosamide was dissolved in TBA, comprising the organic phase. The hydrophilic excipients, mannitol, and leucine were dissolved in water, which formed the aqueous phase. Then, the aqueous and organic phases were mixed as specified in Table 1. Thereafter, the mixed solution was applied as drops onto a rotating cryogenically cooled drum at cooled to −120 °C. The frozen solids were collected with liquid nitrogen and stored in a −80 °C freezer before lyophilization. The lyophilization was performed in a SP VirTis Advantage Pro shelf lyophilizer (SP Industries, Inc., Warminster, PA, USA). The primary drying process was at −40 °C for 20 h, and then, the temperature was linearly increased to 25 °C over 20 h, followed by holding the temperature at 25 °C for 20 h. The pressure was maintained at 100 mTorr during the lyophilization process.

2.3. Aerodynamic particle size distribution analysis

Five milligrams of niclosamide inhalation powder was loaded into size #3 hydroxypropyl methylcellulose capsules (Vcaps® plus, Capsugel®, Lonza, Morristown, NJ, USA). The aerodynamic properties of the powder were evaluated using a Next Generation Impactor (NGI) (MSP Corporation, Shoreview, MN, USA) connected to a High-Capacity Pump (model HCP5, Copley Scientific, Nottingham, UK) and a Critical Flow Controller (model TPK 2000, Copley Scientific, Nottingham, UK). The dry powder inhaler device RS00 (Plastiape®, Osnago, Italy) was used for dispersing the powder through the USP induction port with a total flow rate of 58 L/min for 4.1 s per each actuation corresponding to a 4 kPa pressure drop across the device and a total flow volume of 4 L. To avoid particle bounce, a solution of polysorbate 20 in methanol at 1.5% (w/v) was applied and dried onto the NGI collection plates to coat their surface. The pre-separator was not used in this analysis. After dispersal, the powder was extracted from the stages using a mixture of water/acetonitrile (20:80 v/v). Then, the samples were analyzed by HPLC described below. The analysis was conducted three times (n = 3).

The NGI results were analyzed using the commercial software Copley Inhaler Testing Data Analysis Software 3.10 (CITDAS) (Copley Scientific, Nottingham, UK). CITDAS provided the calculation for mass median aerodynamic diameter (MMAD), total dose per shot, calculated delivered dose, fine particle dose, fine particle fraction of delivered dose (FPF %, delivered dose; the percentage of the total amount of niclosamide with an aerodynamic diameter below 5 μm over the total emitted dose, and geometric standard deviation (GSD).

The fine particle fraction of the recovered dose (FPF %, recovered dose) was calculated as the percentage of the total amount of niclosamide with an aerodynamic diameter below 5 μm over the total amount of niclosamide collected (capsule + device + mouthpiece adapter + induction port to the micro-orifice collector (MOC)). Total dose per actuation is the total amount of niclosamide collected after performing NGI. The calculated delivered dose (i.e., emitted dose) is the amount of drug collected from the throat (mouthpiece adapter + induction port) to the MOC. It does not consider the niclosamide retained in the capsule and device after actuation. The fine particle dose is the mass of niclosamide with an aerodynamic diameter below 5 μm.

Table 1
Composition of the inhalation powders made by thin-film freezing and their corresponding aqueous and organic phases used in the process.

Animal model	Composition of inhaled powder made by TFF (%w/w)	Organic phase composition (mg/mL)	Aqueous phase composition (mg/mL)	Organic/Aqueous phase ratio (v/v)
Sprague-Dawley Rat	22% Niclosamide-73% Mannitol-5% Leucine	Niclosamide 1.38 mg/mL	Mannitol 18.25 mg/mL Leucine 1.25 mg/mL	4/1
Syrian golden hamster	1.66% Niclosamide-92.04% Mannitol-6.3% Leucine	Niclosamide 0.10 mg/mL	Mannitol 23.00 mg/mL Leucine 1.58 mg/mL	4/1

2.4. Scanning electron microscopy (SEM)

The TFF powder was placed onto carbon tape and mounted onto aluminum stubs followed by and sputter-coating with platinum/palladium to a thickness of 15 nm (Cressington Scientific Instruments LTd., Watford, UK) before capturing the images using a Zeiss Supra 40 (Carl Zeiss, Oberkochen, Germany).

2.5. Differential scanning calorimetry (DSC)

Analyses were performed using a differential scanning calorimeter model Q20 (TA Instruments, New Castle, DE, USA) operating in ramp DSC mode from 35 °C to 240 °C with a ramp temperature of 10 °C/min and a nitrogen purge of 50 mL/min. Tzero pans and lids were used in the experiment Q20 (TA Instruments, New Castle, DE, USA).

2.6. X-ray powder diffraction (XRD)

The XRD studies were conducted using a Rigaku MiniFlex 600 II (Rigaku Americas, The Woodlands, TX, USA) equipped with primary monochromated radiation (Cu K radiation source, $\lambda = 1.54056$ Å). The 2-theta angle was set at 5–40° (0.02° step, 1°/min, 40 kV, 15 mA).

2.7. HPLC analysis

The samples were measured at 331 nm using a Dionex HPLC system (Thermo Fisher Scientific Inc., Sunnyvale, CA, USA) with a ZORBAX SB-C18 column (4.6 × 250 mm, 5 μm) (Agilent, Palo Alto, CA, USA) at 1 mL/min flow rate. An isocratic method was used with a mobile phase consisting of a formic acid aqueous solution at 0.3% (v/v) and acetonitrile mixed in a 40:60 ratio.

2.8. Multi-dose tolerability and exposure study in rats

A three-day multi-dose tolerability and exposure study was performed in female Sprague-Dawley rats (252.4–279.5 g). The animal study was approved by the University of Texas at Austin Institutional Animal Care and Use Committee (IACUC; Protocol Number: AUP-2019-00253). Prior to dosing the niclosamide inhalation powder to the animals, the powder was sieved using a No. 325 sieve (45 μm aperture) to deaggregate larger particles and prevent the insufflator device from clogging inside. A dry powder insufflator (DP-4; Penn-Century Inc., Philadelphia, PA, USA) was weighed empty and filled with niclosamide inhalation powder enough to release 1 mg of the formulation (equivalent to 220 μg of niclosamide) for each administration. Rats were anesthetized with isoflurane (4% induction, 1-5-2.5% maintenance), the metal tube of the DP-4 device was briefly inserted into the trachea, and the powder was puffed into the lung using an air pump (AP-1 model, Penn-Century Inc., Philadelphia, PA, USA). The device was weighed immediately after the procedure to determine the amount of powder released. The animals received the powder once per day for three consecutive days. Twenty-four hours after the final administration, animals were sacrificed, and blood was drawn using a cardiac puncture and transferred into BD microcontainers® (reference number 365985, Becton Dickinson, Franklin Lakes, NJ, USA) and centrifuged for 1.5 min at 10,000 rpm in order to separate the plasma that was immediately frozen until further analysis using HPLC-mass spectrometry (HPLC-MS). The lung was perfused with phosphate buffer solution (PBS), and the right lobes were removed to determine niclosamide content. Prior to removal, the left lobe of the lung was inflated and fixed with 10% buffered formalin. Left lobe, spleen, liver, and kidneys were submerged in 10% buffered formalin for 1-week prior to histopathologic analysis.

2.9. Quantification of niclosamide in rat's plasma and lung tissue

A plasma calibration curve was prepared by spiking 100 μL of blank plasma with niclosamide standards at concentrations of 0, 5, 10, 50, 100, 500, 1000, and 5000 ng/mL. Samples and calibrators were prepared by adding 10 μL of the internal standard, deuterated phosphatidylethanol 16:0 20:4 (D5-PEth 16:0 20:4), and 1 mL of a 75% MeOH solution. Then, they were then vortexed for 30 min, followed by centrifugation at 3200 g for 30 min. The supernatant was transferred to clean tubes and dried under a gentle stream of nitrogen. Then, the samples and calibrators were resuspended in 1:1 acetonitrile: 0.1% formic acid water solution. Thereafter, the samples were transferred into HPLC vials, and 10 μL were injected into a Shimadzu SIL 20A HT autosampler, LC-20AD pumps, and an AB Sciex API 4000 Qtrap tandem mass spectrometer with turbo ion spray. The LC analytical column was a C18 Excel 3 ACE (3 × 75 mm, 3 μm) (MacMod, Chadds Ford, PA, USA) and was maintained at 25 °C during the measures. Mobile phase A consisted 0.1% formic acid water solution, and mobile phase B consisted of 0.1% formic acid acetonitrile solution. The flow rate was 0.4 mL/min and the gradient was 5% B initially; then, at 1 min after injection it was ramped to 99% B. From 6 min to 8 min, the mobile phase was maintained at 99% B and at 8.1 min was switched immediately back to 5% B, and it was maintained for 2.9 min to equilibrate the column before the next injection. The niclosamide transition was detected at 325 Da (precursor ion), and the daughter ion was detected at 171 Da. The internal standard deuterated phosphatidylethanol (D5-Peth) 16:0 20:4 transition was detected at 728 Da (precursor ion), and the daughter ion was detected at 303 Da.

In the case of lung tissue, the calibration curve was prepared by spiking 100 μL of homogenized blank lung tissue with niclosamide standards at concentrations of 0, 5, 10, 50, and 100 ng/mL. Niclosamide was quantified in mouse lung tissue by weighing out the lung and adding a 10x volume of a 75% methanol solution. Then, the samples and calibrators were homogenized, and 100 μL were combined with 10 μL of the internal standard. Then the samples were vortexed for 30 min and followed the same methodology previously described for plasma samples.

2.10. Histopathology

Fixed tissues were embedded in paraffin prior to cutting into 5 μm sections. Sections were stained with hematoxylin solution for 4 min., washed with water for 10 min, followed by staining with eosin solution. The resulting stained tissue sections were analyzed by microscopy.

2.11. Pharmacokinetic study in Syrian hamsters

A single-dose pharmacokinetic study was performed in female Syrian hamsters. The animal study was approved by the Institutional Animal Care and Use Committee (IACUC; Protocol Number: AUP-2019-0235) from The University of Texas at Austin. Two cohorts of 35 female Syrian hamsters (35–42 days old and the average weight of 108 ± 8 g) were administered 8.7 or 17.4 mg/Kg of niclosamide inhalation powder each (145 and 290 μg/Kg of pure niclosamide, respectively). The powder was manufactured using the same protocol previously described, but the concentration of niclosamide was reduced in the mixture down to 1.66% (w/w) in order to facilitate dosing appropriate amounts relative to the hamster's body weights while meeting the minimum fill weight of the DP-4 insufflator (1 mg). Prior to dosing, the niclosamide inhalation powder was sieved using a No. 200 sieve (75 μm aperture) in order to disaggregate larger particles and prevent the device from clogging during use. Similar to the before-mentioned method for rats, a nose cone was used to administer isoflurane at 4% for the induction of anesthesia and subsequently at 2% for its maintenance. The hamsters were placed on their backs and secured at a 45° using silk. The powder was administered intratracheally using the Penn-Century dry powder insufflator™ DP-4 (Penn-Century Inc., Philadelphia, PA, USA). The device was actuated three times to deliver 200 μL of air per actuation. After the administration of niclosamide inhalation powder, blood samples were collected by cardiac puncture at 0.25, 0.5, 1, 2, 4, 8, and 24 h using five

hamsters for each time point. The samples were added into BD microcontainers® (reference number 365985, Becton Dickinson, Franklin Lakes, NJ, USA) and centrifuged for 3 min at 10,000 rpm in order to separate the plasma that was quantified using HPLC-MS. In the case of lung tissue, the lungs were washed and perfused with PBS, removed, and immediately frozen. Prior to analysis, whole lung tissue was placed into BioStor™ Vials with screw caps (National Scientific Supply, Claremont, CA, USA) with 3.5 g of zirconia/silica beads (BioSpec Products, Bartlesville, OK, USA). The tissue was homogenized at 4,800 rpm for 20 s.

2.12. Quantification of niclosamide in hamster's plasma and lung tissue

The calibrators were prepared by spiking niclosamide standard solutions into blank plasma solutions with a range from 0.1 to 1000 ng/mL. 200 μL of a 100 ng/mL methanolic solution of the internal standard, 13C6 niclosamide (Niclosamide-(2-chloro-4-nitrophenyl-$^{13}C_6$) hydrate, (Sigma-Aldrich, Saint Louis, MO, USA) was added into 200 μL of plasma samples and calibrators. Then, they were vortexed and centrifuged for 15 min at 12,000 rpm. The supernatant was measured by LC/MS/MS analysis. In the case of lung tissue, the calibrators were prepared by spiking niclosamide standard solutions into blank lung tissue in the range from 0.5 to 10,000 g/mL. 1000 μL of internal standard, 13C6 niclosamide, at 100 ng/mL was added into the weighed lung samples and calibrators. Then, they were vortexed and centrifuged for 15 min at 12,000 rpm. The supernatant was measured by LC/MS/MS analysis. The analysis was performed using Agilent G1367D autosampler, G4220A binary pump, G1316B column compartment, and a G6470A triple quadrupole mass spectrometer. Niclosamide was separated on an Agilent poroshell column 2.1 × 50 mm, 2.7 μm column (Agilent Technologies, Wilmington, DE, USA) using a gradient of 0 to 95% B in 5 min (A = water with 0.025% TFA and B = 95% acetonitrile in water with 0.025% TFA) with a 1-minute hold at the final conditions at a flow rate of 0.35 mL/min. The post run column equilibration was 4 min. The column was held at 40 °C for the analysis. The injection volume for MS was 10 μL. The system was operated in electrospray positive ion detection in Multiple Reaction Monitoring mode for precursor/product ions of niclosamide and the internal standard 13C6 Niclosamide: *m/z* 324.9/171 Da and 330.9/177 Da, respectively.

2.13. Pharmacokinetic analysis

MATLAB® SimBiology (MathWorks, Natick, MA, USA) software was used to run a non-compartmental analysis of the plasma and lung samples. In this regard, the niclosamide concentrations from the five animals of every sample point were averaged and considered as a single subject to run the NCA as previously reported in studies with small sample sizes (Mahmood, 2014; Mentré et al., 1995). In order to compare the previously reported IC_{50} and IC_{90} concentration values to the measured lung concentration in μg/g wet tissue, we assumed that the wet tissue has a density of 1 g/mL.

3. Results and discussion

3.1. Thin-film freezing enhanced aerosol performance of niclosamide inhalation powder

The aerosol performance of the niclosamide inhalation powder was determined by NGI, as shown in Table 2. The powder had an FPF (delivered dose) of 86.0 ± 2.7%, which is particularly high when compared with other niclosamide inhalers manufactured by technologies such as spray-drying (Costabile et al., 2015; Ray et al., 2020). Remarkably, the inhaled powder achieved an MMAD of about 1 μm and was able to reach the last stage of the cascade impactor (Fig. 1). Our main objective was to target niclosamide into the deep lung region with our dry powder formulations in order to cover most of the surface potentially infected by SARS-CoV-2, and this formulation warrants further development.

3.2. Solid-state characterization confirmed nanosized niclosamide inhalation powder

The niclosamide inhalation powder was characterized using DSC and XRD (Fig. 2). In general, it was not possible to detect the diffraction peak or thermal events from leucine because it was present in low amounts (<5%) (Newman et al., 2015). In the case of mannitol, the TFF process generated a mixture of polymorphs in which patterns of δ-mannitol and β- mannitol were observed (Cares-Pacheco et al., 2014). The TFF-mannitol was used as reference material, as shown in Fig. 2B. In the DSC, a transition was observed between 110 and 140 °C, which was previously reported by Peters et al. (2016) and Burger et al. (2000) (Burger et al., 2000; Peters et al., 2016). This endothermic transition is related to the conversion of δ-mannitol into endothermic α-, β or eutectic combinations of both polymorphs of mannitol, followed by melting at ~172 °C. It is important to mention that depending on the freezing/drying conditions and the presence of other excipients, different polymorphs of mannitol and its mixtures can be generated (Liao et al., 2007; Mehta et al., 2013).

In the case of niclosamide, there was a shift in its melting peak from 230 °C to ~218 °C. We attributed this behavior to the nanonization of niclosamide crystals by TFF processing supported by the scanning electron microscopy image (Fig. 3)(Moon et al., 2019). It is reported that nanomaterials exhibit changes in their thermograms, usually manifested as a shift of their melting point to lower temperatures, peak broadening, and even a reduction of their melting enthalpy (Patel et al., 2019).

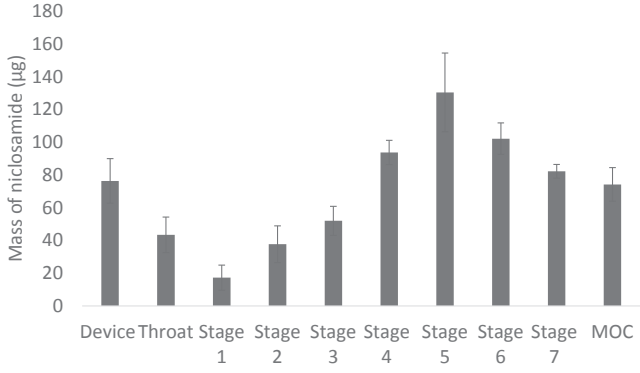

Fig. 1. Aerodynamic particle size distribution of niclosamide inhalation powder (n = 3) made by thin-film freezing. The device bar indicates the remaining mass of niclosamide in the capsule and device. In the case of the throat bar, it indicates the remaining mass of niclosamide in the mouthpiece adapter and induction port.

Table 2
Aerosol performance of niclosamide inhalation powder administered to rats.

Total Dose Per Shot [μg]	Calc Delivered Dose [μg]	Fine Particle Dose [μg]	Fine Particle Fraction [%, delivered dose]	Fine Particle Fraction (%, recovered dose)	MMAD [μm]	GSD
709.6 (41.1)	633.2 (53.5)	543.5 (31.0)	86.0 (2.7)	76.6 (1.4)	1.11 (0.07)	2.84 (0.22)

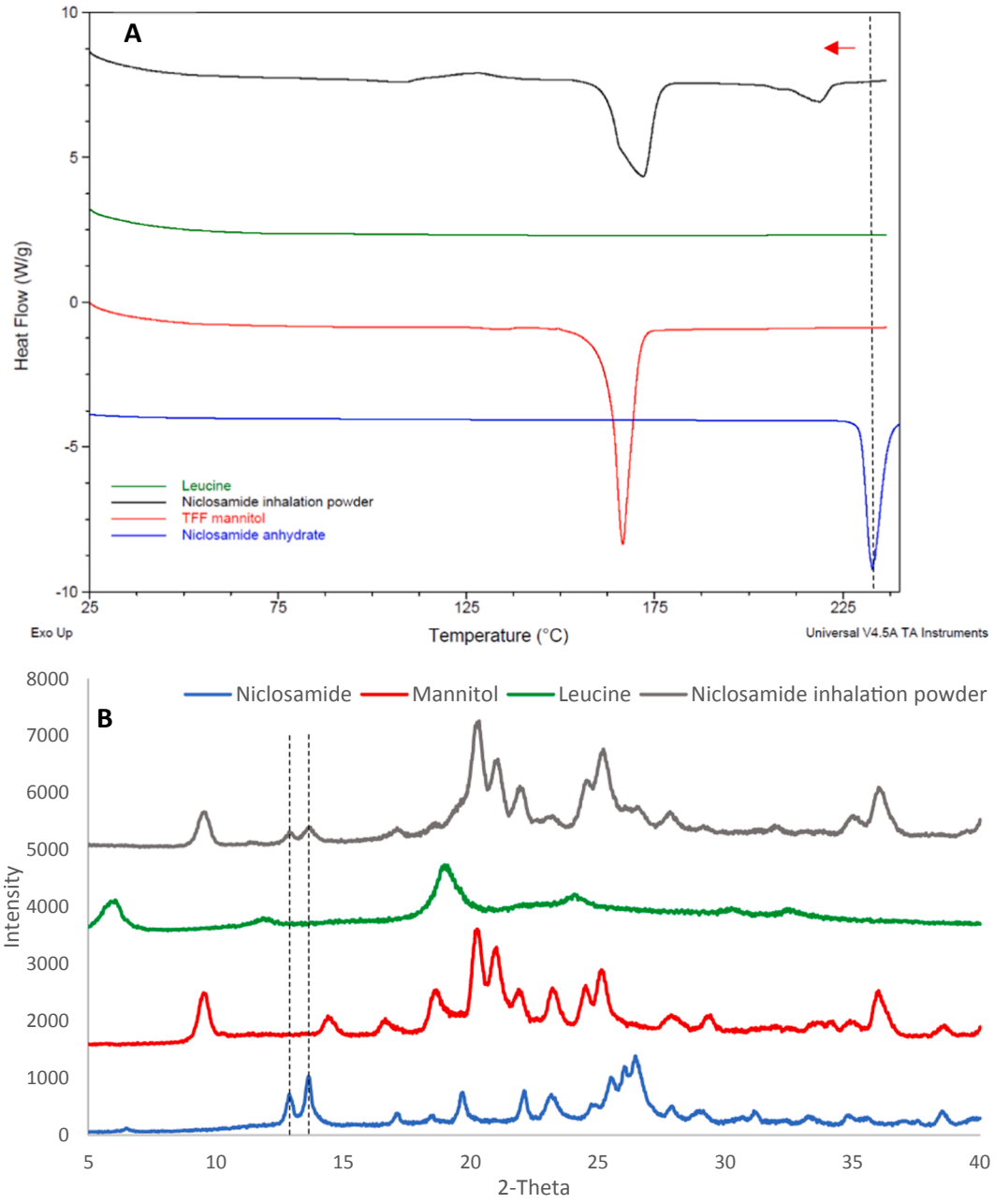

Fig. 2. (A) DSC thermogram and (B) XRD diffractogram of niclosamide inhalation powder and its separated constituents. In the thermogram (see, 2A), the dotted line and red arrow indicate the peak shift of niclosamide melting point. In the case of the diffractogram (see, 2B), the dotted lines indicate characteristic peaks of niclosamide anhydrate.

3.3. Multi-dose administration of niclosamide inhalation powder showed mild pulmonary toxicity in rats

We performed a multi-dose tolerability and exposure on inhaled niclosamide for the purpose of obtaining information on the potential toxicology of inhaled niclosamide after administration of a relatively high dose (~827.2 μg/Kg of niclosamide contained in the TFF inhalation powder described in Table 1 for rats). The results of the plasma and lung concentrations of niclosamide are provided in Table 3. The amount of niclosamide in the lungs at 24 h following administration of the last dose was undetectable in two out of five rats and less than 1 ng/mL in all five of the tested rats. Concentrations in the ng/mL range were still detected in the rat plasma samples from four out of five rats. All rats survived between administration and sample collection.

The histopathological examination of the liver, kidney, and spleen from the treated rats appeared normal. However, examination of the lung tissue indicated mild signs of inflammation after daily dosing for three days, which is likely related to the relatively high doses of niclosamide inhalation powder that were administered (niclosamide, leucine, and mannitol). In all animals, the air space and interstitial space were found to be normal. The examination also indicated a few to moderate eosinophils in the lung tissue with rare to scattered polymorphonuclear (PMN) cells observed. This was accompanied by some bronchitis in most of the rats. The specific findings in each animal are presented in Table 4. A representative image from Rat 4 is provided in Fig. 5, depicting normal alveoli (Fig. 4A) and some bronchial inflammation (Fig. 4B) with mixed granulocyte and eosinophils present. In one animal, Rat 3, all findings were normal.

Chang et al. (2006) reported a $T_{1/2}$ of 6.0 ± 0.8 h for solubilized niclosamide after oral administration (Chang et al., 2006). Based on the

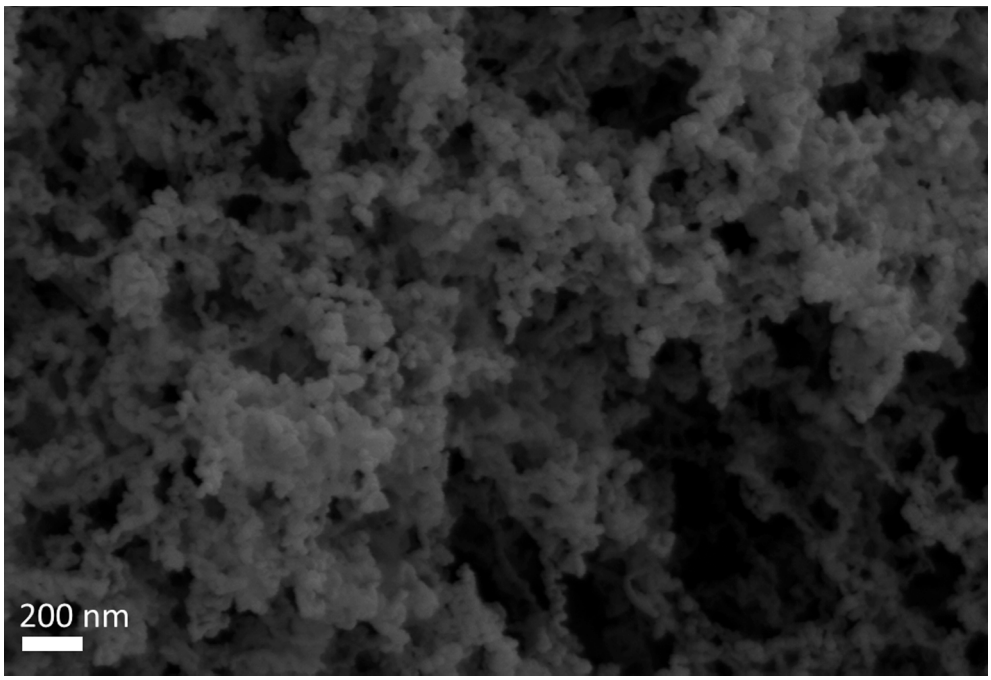

Fig. 3. SEM picture of niclosamide inhalation powder. The bar shows a size of 200 nm.

Table 3
Concentration of niclosamide in the plasma and lungs of Sprague-Dawley rats after three days of daily dosing of niclosamide inhalation powder (200 μg of niclosamide daily per animal, ~827.22 μg/Kg). The limit of quantification in plasma samples was 1 ng/mL and 1 pg/mg in lung tissue.

Animal	Plasma concentration (ng/mL)	Lung Concentration (pg/mg)
Rat 1	3.89	204.57
Rat 2	3.37	29.71
Rat 3	1.89	20.46
Rat 4	14.6	<1
Rat 5	<1	<1

Table 4
Histopathology observations in each of the treated Sprague-Dawley Rats after three days of dosing niclosamide inhalation powder (200 μg/niclosamide administered daily per animal).

Animal	Histopathological Findings
Rat 1	Air space and interstitial space normal; normal kidney, liver, and spleen; bronchovascular bundle with moderate eosinophils with admixed PMNs. Large airways > small airways with mild-moderate bronchitis.
Rat 2	Air space and interstitial space normal; normal kidney, liver, and spleen; parabronchial eosinophils only in the large airways; otherwise predominantly normal.
Rat 3	Air space and interstitial space normal; normal kidney, liver, and spleen; lungs normal.
Rat 4	Air space and interstitial space normal; normal kidney, liver, and spleen; some eosinophilic bronchitis; scattered PMN with patches of bronchitis among some normal airways.
Rat 5	Air space and interstitial space normal; normal kidney, liver, and spleen; moderate eosinophilic bronchitis with few PMNs.

measured niclosamide concentrations in Sprague-Dawley rat plasma from Table 4 after 24 h following administration, which was approximately four times the reported half-life, the pulmonary administration appears to have made a difference in systemic exposure kinetics since it was possible to detect and quantify niclosamide in rat plasma at 24 h following dosing. Moreover, our group recently reported that the oral administration of niclosamide suspension had a $T_{1/2}$ of approximately 1.0 ± 0.3 h in Wistar rats (Jara et al., 2021). The observed difference in systemic exposure kinetics may be attributed to an extended residence time in the lung resulting from the avoidance of the extensive first-pass effect that niclosamide undergoes after oral administration (Fan et al., 2019). Despite the fact that some drug remains in the plasma, limited niclosamide concentrations in lung tissue following three consecutive days of daily dosing were observed (Table 4).

Costabile et al. 2015 performed an acute lung toxicity study of niclosamide nanosuspensions (containing mannitol) in Wistar rats (200 and 220 g). They did not report acute toxicity after intratracheal administration of the niclosamide nanosuspension at doses ranging from 10 to 100 μg per animal (Costabile et al., 2015). In our work, the Sprague-Dawley rats (252.4 – 279.5 g) were administered 200 μg/rat daily for three days, and some signs of mild to moderate inflammation were observed. The mild to moderate inflammation of the bronchioles along with the presence of eosinophils at this dose is a promising sign and currently unclear if these observations result from niclosamide or the mannitol excipient in the formulation, which is reported to cause bronchospasm when administered at high milligram doses in humans (Sahakijpijarn et al., 2020).

3.4. Administration of niclosamide inhalation powder sustained lung concentrations above SARS-CoV-2 IC_{50} in the Syrian Golden Hamster model

The in vivo pharmacokinetics and toxicology study of niclosamide inhalation powder in rats at the dose of ~827.2 μg/Kg confirmed the feasibility of the formulation to be translated to a COVID-19 infection model. The Syrian golden hamster model is relevant for SARS-CoV-2 infection, and a complete pharmacokinetic analysis is required in order to evaluate the proper dosing for further efficacy studies (Chan et al., 2020; Imai et al., 2020). The hamsters were administered niclosamide inhalation powder prepared at a lower niclosamide concentration in order to have a dose of 145 and 290 μg/kg niclosamide. As can be seen in Fig. 5, there was fast absorption of niclosamide that was rapidly cleared to steady low levels; in general, this is considered an advantage of inhaled drug products in terms of safety and reduction of systemic side effects (Borghardt et al., 2015). A non-compartmental analysis of the plasma data was performed; the calculated pharmacokinetic parameters are shown in Table 5. This analysis showed dose

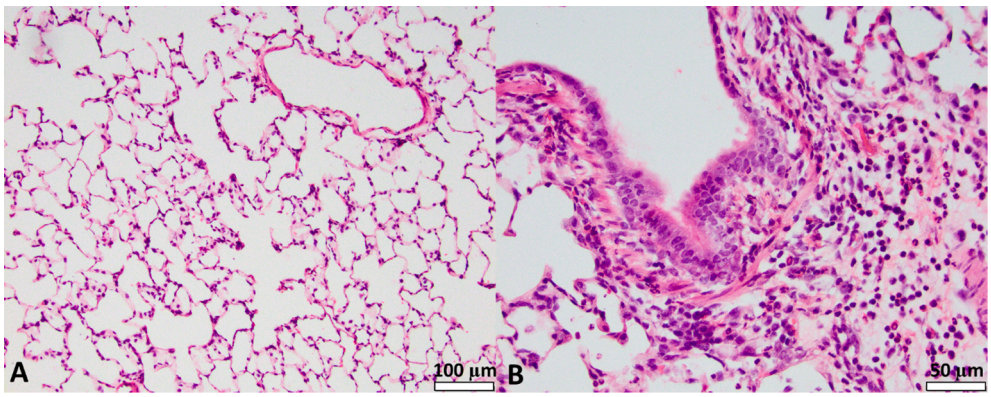

Fig. 4. (A) Histopathological examination of lung tissue showing normal alveolar region at a magnification of 100x. The bar shows a size of 100 µm. (B) Bronchial inflammation of a 1 mm airway section in Rat 4 after three days of dosing niclosamide inhalation powder (200 µg of niclosamide per animal). The bar shows a size of 50 µm.

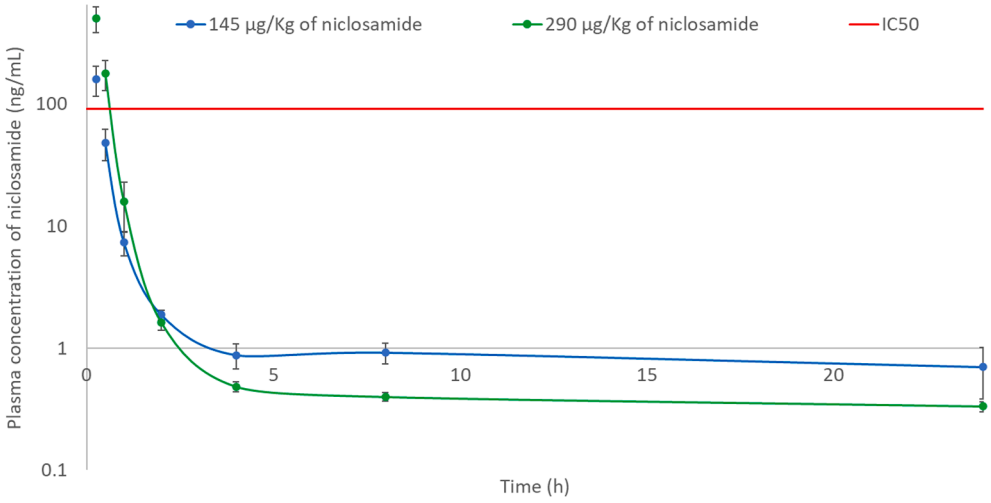

Fig. 5. Plasma concentration profile of niclosamide after the administration of niclosamide inhalation powder in Syrian hamsters (n = 5 for each point). The groups received 8.7 (blue) and 17.4 (green) mg/Kg of niclosamide inhalation powder, containing a dose of 145 and 290 µg/Kg of niclosamide, respectively. Niclosamide IC_{50} for SARS-CoV-2 is 0.28 µM (91.56 ng/mL) (red)(Jeon et al., 2020).

Table 5
Plasma in vivo pharmacokinetic parameters of niclosamide inhalation powder in two groups of Syrian hamsters. The groups received 8.7 and 17.4 mg/Kg of niclosamide inhalation powder (described in Table 1 for Syrian golden hamsters), containing a dose of 145 and 290 µg/Kg of niclosamide, respectively.

Pharmacokinetic parameters	Niclosamide dose of 145 µg/Kg	Niclosamide dose of 290 µg/Kg
$T_{max\ (h)}$	0.25	0.25
$C_{max\ (ng/mL)}$	159.0	590.3
$AUC_{last\ (h*ng/mL)}$	83.8	237.1
$CL_{\ (mL/h)}$	116.8	119.4

proportionality between the doses as evidenced by the AUC/dose of both administered doses are similar (8.6 and 8.4), and clearance was in the range of ~116–119 mL/h. All hamsters survived between administration and sample collection.

Furthermore, in the lung tissue (Fig. 6), a similar trend was observed, and the steady-state level of niclosamide exceeded the IC_{50} for at least 24 h. Unfortunately, the lung concentration profile was not possible to determine using the non-compartmental analysis model, probably due to the inability to observe the elimination phase of niclosamide in lung tissue between 4 and 24 h. Therefore the only parameters reported are C_{max}, $AUC_{\ 0\text{-}24h}$, and T_{max} (Table 6).

After the 2 h measurement, the plasma concentration remained relatively constant, but there was a notable difference in the concentrations achieved by the two different administered doses in terms of the concentrations reached in the lungs after 2 h. Unexpectedly, the lower administered dose had a higher $AUC_{0\text{-}24h}$ without achieving a higher C_{max}. We hypothesize that the administration of a higher dose of powder caused a change in aerosolization properties from the dry powder insufflator used to administer the dose of powder to the hamsters. Molina et al. (2016) compared different methods of pulmonary administration of nanoparticles, and they found that with dry powder insufflation, the nanoparticles were cleared faster from the respiratory tract because the powder was deposited in the larger airways and trachea with higher variability among the animals (i.e., 188%). Moreover, they detected higher amounts of their formulation in the gastrointestinal tract, suggesting mucociliary clearance from the upper respiratory tract. They speculated that the deposition in the trachea was related to issues in the synchronization between the insufflation and the inhalation cycle of the animals and not due to properties of the drug (Molina et al., 2016). The work of Duret et al. (2012) confirms that the DP-4 M® insufflator (used in this study) is reliable for delivering different drug doses of the same powder in mice, but unfortunately, in their work, the animals were immediately sacrificed to measure drug deposition (Duret et al., 2012). So, no relationship between deposition in different regions of the lungs and their effect on pharmacokinetics was established. Moreover,

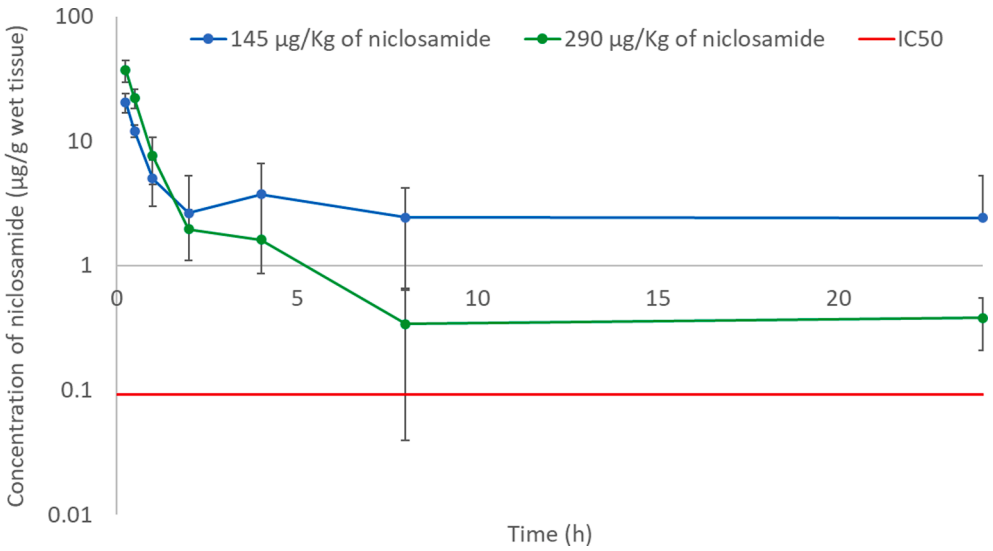

Fig. 6. Lung concentration profile of niclosamide after the administration of niclosamide inhalation powder to Syrian golden hamsters (n = 5). The groups received 8.7 (blue) and 17.4 (green) mg/Kg of niclosamide inhalation powder, containing a dose of 145 and 290 µg/Kg of niclosamide, respectively. Estimated niclosamide IC_{50} for SARS-CoV-2 is 0.09156 µg/g of wet tissue (red), it was assumed that the wet tissue has a density of 1 g/mL .

Table 6
Lung in vivo pharmacokinetic parameters of niclosamide inhalation powder in two groups of Syrian hamsters (described in Table 1 for Syrian golden hamsters). The groups received 8.7 and 17.4 mg/Kg of niclosamide inhalation powder, containing a dose of 145 and 290 µg/Kg of niclosamide, respectively.

Pharmacokinetic parameters	Niclosamide dose of 145 µg/Kg	Niclosamide dose of 290 µg/Kg
$T_{max\ (h)}$	0.25	0.25
$C_{max\ (µg/g\ of\ wet\ tissue)}$	20.5	37.2
$AUC_{last\ (h*µg/g\ of\ wet\ tissue)}$	72.1	37.5

Hoppentocht et al. (2014) proved that the insufflator is not consistent or efficient in deaggregating powders using 200 µL of air pulsed at different doses (Hoppentocht et al., 2014).

Based on these reports of using dry powder insufflators in animal studies, the differences observed between the dose amounts administered in our study and the expected lung pharmacokinetics is likely related to the efficiency of deaggregation of the two-dose amounts delivered from the dry powder insufflator and not related to niclosamide itself. This is because changes in powder deposition caused by the insufflator can lead to different emitted particle sizes from the device and subsequent different dissolution/solubility of the emitted particles, mechanisms of clearance, and drug permeation (Bhagwat et al., 2017). The C_{max} of niclosamide following dosing by insufflation to the lungs is nearly doubled as the dose was doubled, which agrees with the studies that showed that the insufflator is reliable for delivering the loaded dose (Duret et al., 2012). However, it is known that particles deposited in the trachea and larger airways are cleared faster (Tonnis et al., 2014). This is supported by the plasma $AUC_{0\text{-}24h}$ that was more than double when the dose was doubled. So, a greater amount of niclosamide from the powder formulation was absorbed and cleared by the plasma instead of being retained in the lung tissue (Table 5). Huang et al. (2018) used the co-efficient C_{lung}/C_{plasma} to describe the biodistribution of an itraconazole

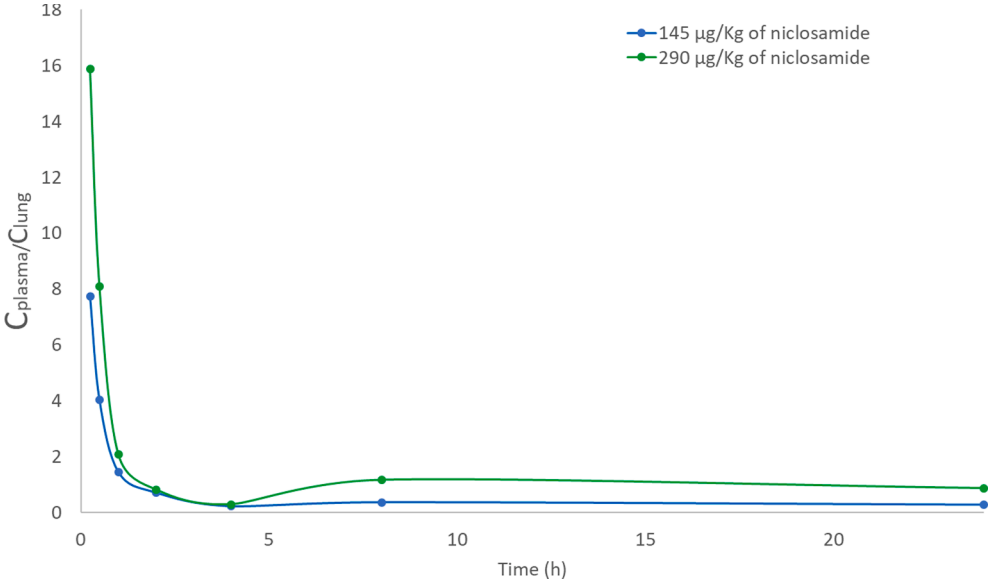

Fig. 7. Coefficient of niclosamide concentration in plasma and lung over time (C_{plasma}/C_{lungs}). The groups received 8.7 (blue) and 17.4 (green) mg/Kg of niclosamide inhalation powder, containing a dose of 145 and 290 µg/Kg of niclosamide, respectively.

dry powder inhalation product in a pharmacokinetic study (Huang et al., 2018). Due to the differences in concentrations from Huang *et al.*, we used the reciprocal coefficient, C_{plasma}/C_{lung} to describe the distribution between plasma and lungs, aiming to facilitate the comparison of niclosamide's lung-plasma distribution achieved by both doses. In an ideal scenario, the C_{plasma}/C_{lung} ratio should remain mostly unchanged if the deposition pattern is consistent between doses. As can be seen in Fig. 7, niclosamide inhalation powder behaves differently after being administered at two different dose amounts to the hamsters; a greater amount of the drug was detected in plasma than in lungs after increasing the administered dose (higher C_{plasma}/C_{lung}). This supports our argument that at the higher dose amounts loaded and delivered from the dry powder insufflator, the insufflated powder was likely deposited in the larger airways, which can impact the pharmacokinetics of the administered dry powder by increasing the clearance of particles (Kukut Hatipoglu et al., 2018). The concentrations achieved after the 2 h measurement can be related to the smaller particle size fraction of niclosamide inhalation powder. It has been described that smaller particles are able to reach the deep lungs, where they are cleared more slowly than the upper regions of the lungs (Carvalho et al., 2011). Once the particles are dissolved, niclosamide undergoes extensive metabolism by Cytochrome P450 and UDP-glucuronosyltransferase enzymes (especially CYP1A2 and UGT1A1), which their abundance and location vary among different organs and animal species. (Fan et al., 2019; Lu et al., 2016). In general, niclosamide's phenol group is the primary target for glucuronidation in the liver and intestine, which is the main metabolic pathway limiting its repurposing (Fan et al., 2019; Mook et al., 2015). Chen et al. (1998) reported that CYPA1 enzymes are present in hamster's lungs and liver. They speculated that the CYP1A1 and CYP1A2 are mainly present in the lungs and the liver, respectively (Chen et al., 1998). In humans, the CYP1A2 enzyme is mainly located in the liver and has 90-fold higher metabolic activity catalyzing the hydroxylation of niclosamide than the CYP1A1 enzyme, which is located in extrahepatic sites (e.g., the lungs). Moreover, Lu et al. (2016) could not measure the metabolic parameters of CYP1A1 because of its low metabolic activity (Lu et al., 2016; Yj et al., 2021). In the case of UGT1A1, Ohno and Nakajin (2009) were unable to quantify the enzyme in human lungs, which is abundant in the human liver and small intestine (Ohno and Nakajin, 2009). Unfortunately, we could not find evidence in the literature about the different forms of UGTs in hamster's organs. In summary, the main mechanisms of clearance for niclosamide inhalation powder are those related to the initial removal of the particles (e.g., mucociliary clearance). It seems that niclosamide's metabolization in the lungs of hamsters is limited due to the affinity of the enzymes towards the drug, explaining why the concentration was relatively constant after 8 h (Fig. 6).

To the best of our knowledge, the present work is the first describing the pharmacokinetics of niclosamide following delivery to the lungs. It is relevant and informative to compare our results to pharmacokinetic studies reported that delivered niclosamide by other routes of administration and animal model. Ye et al. (2015) administered niclosamide intravenously (2 mg/Kg) through the jugular vein to Sprague–Dawley rats using a mixture of solvents and measured the drug's biodistribution in the liver, heart, spleen, lungs, kidneys, and intestines. The concentration in the lungs and heart were consistently the lowest based on intravenous delivery (Ye et al., 2015). Tao *et al.* (2014) reported the concentrations of niclosamide in male C57BL/6J mice after oral administration of niclosamide ethanolamine at 40 mg/Kg. In their work, the lung concentrations following oral administration were decreased from 87.2 ± 70, 23.8 ± 13, and 13.3 ± 5 ng/g at 2, 4, and 8 h, respectively. Interestingly, the ethanolamine salt form of niclosamide mainly distributed to the liver, and higher levels of metabolites were detected in the kidneys. Therefore, neither intravenously administered niclosamide nor orally administered niclosamide ethanolamine provided therapeutically relevant lung levels of niclosamide, thus emphasizing the importance of the inhaled route of administration of niclosamide directly to the lungs for lung infections like SARS-CoV-2.

By considering the differences in animal models, Fig. 6 shows that it is possible to achieve lung concentrations mostly in the μg/g scale and above the IC_{50} using lower doses just in the range of μg/Kg for at least 24 h because the drug was targeted directly into the lungs. The development of niclosamide inhalation powder avoids first-pass metabolism and reduces the exposure of the drug to being metabolized by hydroxylation and glucuronidation (Lu et al., 2016).

Finally, in further considering administration to infected patients, the inhaled niclosamide powder should also achieve concentrations above the IC_{90}. In our hamster studies, we administered a TFF inhaled powder formulation containing a reduced amount of niclosamide (i.e., 1.66% (w/w) dosed at 145 and 290 μg/Kg to hamsters compared to 22% (w/w) dosed at 827.22 μg/Kg to rats). Based on the reported inhibitory effect of niclosamide on SARS-CoV-2 and an IC_{50} of 91.56 ng/mL (0.28 μM) following the work of Jeon et al. (2020), Arshad et al. (2020) estimated the IC_{90} of 153.7 ng/mL (the paper considered $IC_{50} = EC_{50}$). To be truly useful as a therapeutic against SARS-CoV-2, the niclosamide inhalation powder should achieve a concentration higher than 0.154 μg/g, assuming that the wet tissue has a density of 1 g/mL (assumed to be equal to the density of water). We exceeded this concentration in lung tissue using both administered doses by more than 2-fold over the 24 h period (the lower dose was ~15-fold) as seen in Table 6. Further supporting our analysis, comparisons with the report of Gassen et al. (2020) is helpful. The paper reports an IC_{50} of 55.6 ng/mL (0.17 μM) (Gassen et al., 2020). Therefore, niclosamide inhalation powder is also above this concentration. Additionally, the toxicology studies support that niclosamide inhalation powder has a sufficient safety margin for dose adjustment, thus allowing for a once per day inhalation therapy.

4. Conclusion

Using thin-film freezing, we report the administration of niclosamide inhalation powder to rats and Syrian golden hamsters. The TFF powders have remarkable aerosol properties for targeting the lungs, and especially, the lower respiratory tract. The niclosamide inhalation powder was demonstrated to be safe after pulmonary administration in the rat model, and the pharmacokinetics study in Syrian golden hamsters, an important animal model for SARS-CoV-2 infection, showed that the drug remains in the lungs for at least 24 h at concentrations greater than the reported IC_{50} and IC_{90} for SARS-CoV-2 after just a single inhaled dose administered by inhalation.

Funding

This research was funded by TFF Pharmaceuticals, Inc. through a sponsored research agreement with the University of Texas at Austin. Warnken is partially supported by this sponsored research agreement with TFF Pharmaceuticals Inc. Miguel O. Jara acknowledges the funding support from the Equal Opportunities Fulbright—CONICYT Scholarship 56170009.

CRediT authorship contribution statement

Miguel O. Jara: Conceptualization, Methodology, Validation, Investigation, Data curation, Writing - original draft, Writing - review & editing, Visualization. **Zachary N. Warnken:** Conceptualization, Methodology, Validation, Investigation, Data curation, Writing - review & editing. **Sawittree Sahakijpijarn:** Validation, Investigation. **Chaeho Moon:** Validation, Investigation. **Esther Y. Maier:** Methodology, Investigation, Writing - review & editing. **Dale J. Christensen:** Conceptualization, Visualization, Writing - review & editing. **John J. Koleng:** Conceptualization, Methodology. **Jay I. Peters:** Methodology, Resources. **Sarah D. Hackman Maier:** Methodology, Investigation, Writing - review & editing. **Robert O. Williams:** Conceptualization, Methodology, Resources, Writing - review & editing, Supervision,

Project administration, Funding acquisition. : .

Declaration of Competing Interest

The authors declare the following financial interests/personal relationships which may be considered as potential competing interests: Jara, Warnken, Moon, Sahakijpiarn and Williams are co-inventors on IP related to this paper. The University of Texas System has licensed this IP to TFF Pharmaceuticals, Inc. Williams, Moon and Sahakijpijarn acknowledge consulting for TFF Pharmaceuticals, Inc. Williams owns equity in TFF Pharmaceuticals, Inc. Peters is a consultant to TFF Pharmaceuticals, Inc. (uncompensated)..

References

AboulFotouh, K., Zhang, Y., Maniruzzaman, M., Williams, R.O., Cui, Z., 2020. Amorphous solid dispersion dry powder for pulmonary drug delivery: advantages and challenges. Int. J. Pharm. 587, 119711. https://doi.org/10.1016/j.ijpharm.2020.119711.

Almansour, K., Alfagih, I.M., Ali, R., Elsayed, M.M.A., 2020. Inhalable microparticles containing terbinafine for management of pulmonary fungal infections: spray drying process engineering using lactose vs. mannitol as excipients. J. Drug Deliv Sci. Technol. 60, 101991. https://doi.org/10.1016/j.jddst.2020.101991.

Arshad, U., Pertinez, H., Box, H., Tatham, L., Rajoli, R.K.R., Curley, P., Neary, M., Sharp, J., Liptrott, N.J., Valentijn, A., David, C., Rannard, S.P., O'Neill, P.M., Aljayyoussi, G., Pennington, S.H., Ward, S.A., Hill, A., Back, D.J., Khoo, S.H., Bray, P. G., Biagini, G.A., Owen, A., 2020. Prioritization of anti-SARS-Cov-2 drug repurposing opportunities based on plasma and target site concentrations derived from their established human pharmacokinetics. Clin. Pharmacol. Ther. 108, 775–790. https://doi.org/10.1002/cpt.1909.

Barbosa, E.J., Löbenberg, R., de Araujo, G.L.B., Bou-Chacra, N.A., 2019. Niclosamide repositioning for treating cancer: Challenges and nano-based drug delivery opportunities. Eur. J. Pharm. Biopharm Off. J. Arbeitsgemeinschaft Pharm. Verfahrenstechnik EV 141, 58–69. https://doi.org/10.1016/j.ejpb.2019.05.004.

Beinborn, N.A., Du, J., Wiederhold, N.P., Smyth, H.D.C., Williams, R.O., 2012. Dry powder insufflation of crystalline and amorphous voriconazole formulations produced by thin film freezing to mice. Eur. J. Pharm. Biopharm Off. J. Arbeitsgemeinschaft Pharm. Verfahrenstechnik EV 81, 600–608. https://doi.org/10.1016/j.ejpb.2012.04.019.

Bhagwat, S., Schilling, U., Chen, M.-J., Wei, X., Delvadia, R., Absar, M., Saluja, B., Hochhaus, G., 2017. Predicting pulmonary pharmacokinetics from in vitro properties of dry powder inhalers. Pharm. Res. 34, 2541–2556. https://doi.org/10.1007/s11095-017-2235-y.

Borghardt, J.M., Weber, B., Staab, A., Kloft, C., 2015. Pharmacometric models for characterizing the pharmacokinetics of orally inhaled drugs. AAPS J. 17, 853–870. https://doi.org/10.1208/s12248-015-9760-6.

Burger, A., Henck, J.-O., Hetz, S., Rollinger, J.M., Weissnicht, A.A., Stöttner, H., 2000. Energy/temperature diagram and compression behavior of the polymorphs of d-mannitol. J. Pharm. Sci. 89, 457–468. https://doi.org/10.1002/(SICI)1520-6017(200004)89:4<457::AID-JPS3>3.0.CO;2-G.

Cares-Pacheco, M.G., Vaca-Medina, G., Calvet, R., Espitalier, F., Letourneau, J.-J., Rouilly, A., Rodier, E., 2014. Physicochemical characterization of d-mannitol polymorphs: the challenging surface energy determination by inverse gas chromatography in the infinite dilution region. Int. J. Pharm. 475, 69–81. https://doi.org/10.1016/j.ijpharm.2014.08.029.

Carvalho, T.C., Peters, J.I., Williams, R.O., 2011. Influence of particle size on regional lung deposition – what evidence is there? Int. J. Pharm. 406, 1–10. https://doi.org/10.1016/j.ijpharm.2010.12.040.

Chan, J.F.-W., Zhang, A.J., Yuan, S., Poon, V.K.-M., Chan, C.C.-S., Lee, A.C.-Y., Chan, W.-M., Fan, Z., Tsoi, H.-W., Wen, L., Liang, R., Cao, J., Chen, Y., Tang, K., Luo, C., Cai, J.-P., Kok, K.-H., Chu, H., Chan, K.-H., Sridhar, S., Chen, Z., Chen, H., To, K.K.-W., Yuen, K.-Y., 2020. Simulation of the Clinical and Pathological Manifestations of Coronavirus Disease 2019 (COVID-19) in a golden syrian hamster model: implications for disease pathogenesis and transmissibility. Clin. Infect. Dis. ciaa325 https://doi.org/10.1093/cid/ciaa325.

Chang, Y.-W., Yeh, T.-K., Lin, K.-T., Chen, W.-C., Yao, H.-T., Lan, S.-J., Wu, Y.-S., Hsieh, H.-P., Chen, C.-M., Chen, C.-T., 2006. Pharmacokinetics of anti-SARS-CoV agent niclosamide and its analogs in rats. J. Food Drug Anal. 14, 6.

Chen, R.-M., Chou, M.W., Ueng, T.-H., 1998. Induction of cytochrome P450 1A in hamster liver and lung by 6-nitrochrysene. Arch. Toxicol. 72, 395–401. https://doi.org/10.1007/s002040050519.

Chu, H., Chan, J.F.-W., Wang, Y., Yuen, T.T.-T., Chai, Y., Hou, Y., Shuai, H., Yang, D., Hu, B., Huang, X., Zhang, X., Cai, J.-P., Zhou, J., Yuan, S., Kok, K.-H., To, K.K.-W., Chan, I.H.-Y., Zhang, A.J., Sit, K.-Y., Au, W.-K., Yuen, K.-Y., 2020. Comparative replication and immune activation profiles of SARS-CoV-2 and SARS-CoV in human lungs: an Ex Vivo study with implications for the pathogenesis of COVID-19. Clin. Infect. Dis. Off. Publ. Infect. Dis. Soc. Am. 71, 1400–1409. https://doi.org/10.1093/cid/ciaa410.

Costabile, G., d'Angelo, I., Rampioni, G., Bondì, R., Pompili, B., Ascenzioni, F., Mitidieri, E., di Villa, d'Emmanuele, Bianca, R., Sorrentino, R., Miro, A., Quaglia, F., Imperi, F., Leoni, L., Ungaro, F., 2015. Toward repositioning niclosamide for antivirulence therapy of pseudomonas aeruginosa lung infections: development of inhalable formulations through nanosuspension technology. Mol. Pharm. 12, 2604–2617. https://doi.org/10.1021/acs.molpharmaceut.5b00098.

Damiani, S., Fiorentino, M., Palma, A.D., Foschini, M.P., Lazzarotto, T., Gabrielli, L., Viale, P.L., Attard, L., Riefolo, M., D'Errico, A., 2021. Pathological post-mortem findings in lungs infected with SARS-CoV-2. J. Pathol. 253, 31–40. https://doi.org/10.1002/path.5549.

Duret, C., Wauthoz, N., Merlos, R., Goole, J., Maris, C., Roland, I., Sebti, T., Vanderbist, F., Amighi, K., 2012. In vitro and in vivo evaluation of a dry powder endotracheal insufflator device for use in dose-dependent preclinical studies in mice. Eur. J. Pharm. Biopharm. 81, 627–634. https://doi.org/10.1016/j.ejpb.2012.04.004.

Fan, X., Li, H., Ding, X., Zhang, Q.-Y., 2019. Contributions of hepatic and intestinal metabolism to the disposition of niclosamide, a repurposed drug with poor bioavailability. Drug Metab. Dispos. 47, 756–763. https://doi.org/10.1124/dmd.119.086678.

Gassen, N.C., Niemeyer, D., Muth, D., Corman, V.M., Martinelli, S., Gassen, A., Hafner, K., Papies, J., Mösbauer, K., Zellner, A., Zannas, A.S., Herrmann, A., Holsboer, F., Brack-Werner, R., Boshart, M., Müller-Myhsok, B., Drosten, C., Müller, M.A., Rein, T., 2019. SKP2 attenuates autophagy through Beclin1-ubiquitination and its inhibition reduces MERS-Coronavirus infection. Nat. Commun. 10, 1–16. https://doi.org/10.1038/s41467-019-13659-4.

Gassen, N.C., Papies, J., Bajaj, T., Dethloff, F., Emanuel, J., Weckmann, K., Heinz, D.E., Heinemann, N., Lennarz, M., Richter, A., Niemeyer, D., Corman, V.M., Giavalisco, P., Drosten, C., Müller, M.A., 2020. Analysis of SARS-CoV-2-controlled autophagy reveals spermidine, MK-2206, and niclosamide as putative antiviral therapeutics. bioRxiv 2020.04.15.997254. https://doi.org/10.1101/2020.04.15.997254.

Guan, W., Ni, Z., Hu, Yu., Liang, W., Ou, C., He, J., Liu, L., Shan, H., Lei, C., Hui, D.S.C., Du, B., Li, L., Zeng, G., Yuen, K.-Y., Chen, R., Tang, C., Wang, T., Chen, P., Xiang, J., Li, S., Wang, Jin-lin, Liang, Z., Peng, Y., Wei, L., Liu, Y., Hu, Ya.-hua., Peng, P., Wang, Jian-ming, Liu, J., Chen, Z., Li, G., Zheng, Z., Qiu, S., Luo, J., Ye, C., Zhu, S., Zhong, N., 2020. Clinical characteristics of coronavirus disease 2019 in China. N. Engl. J. Med. 382, 1708–1720. https://doi.org/10.1056/NEJMoa2002032.

Gurwitz, D., 2020. Angiotensin receptor blockers as tentative SARS-CoV-2 therapeutics. Drug Dev. Res. 81, 537–540. https://doi.org/10.1002/ddr.21656.

Hoppentocht, M., Hoste, C., Hagedoorn, P., Frijlink, H.W., de Boer, A.H., 2014. In vitro evaluation of the DP-4M PennCentury™ insufflator. Eur. J. Pharm. Biopharm. 88, 153–159. https://doi.org/10.1016/j.ejpb.2014.06.014.

Huang, Z., Lin, L., McGoverin, C., Liu, H., Wang, L., Zhou, Q. (Tony), Lu, M., Wu, C., 2018. Dry powder inhaler formulations of poorly water-soluble itraconazole: a balance between in-vitro dissolution and in-vivo distribution is necessary. Int. J. Pharm. 551, 103–110. https://doi.org/10.1016/j.ijpharm.2018.09.018.

Imai, M., Iwatsuki-Horimoto, K., Hatta, M., Loeber, S., Halfmann, P.J., Nakajima, N., Watanabe, T., Ujie, M., Takahashi, K., Ito, M., Yamada, S., Fan, S., Chiba, S., Kuroda, M., Guan, L., Takada, K., Armbrust, T., Balogh, A., Furusawa, Y., Okuda, M., Ueki, H., Yasuhara, A., Sakai-Tagawa, Y., Lopes, T.J.S., Kiso, M., Yamayoshi, S., Kinoshita, N., Ohmagari, N., Hattori, S., Takeda, M., Mitsuya, H., Krammer, F., Suzuki, T., Kawaoka, Y., 2020. Syrian hamsters as a small animal model for SARS-CoV-2 infection and countermeasure development. Proc. Natl. Acad. Sci. 117, 16587–16595. https://doi.org/10.1073/pnas.2009799117.

Jara, M.O., Warnken, Z.N., Williams, R.O., 2021. Amorphous solid dispersions and the contribution of nanoparticles to in vitro dissolution and in vivo testing: niclosamide as a case study. Pharmaceutics 13, 97. https://doi.org/10.3390/pharmaceutics13010097.

Jeon, S., Ko, M., Lee, J., Choi, I., Byun, S.Y., Park, S., Shum, D., Kim, S., 2020. Identification of antiviral drug candidates against SARS-CoV-2 from FDA-approved drugs. Antimicrob. Agents Chemother. https://doi.org/10.1128/AAC.00819-20.

Kukut Hatipoglu, M., Hickey, A.J., Garcia-Contreras, L., 2018. Pharmacokinetics and pharmacodynamics of high doses of inhaled dry powder drugs. Int. J. Pharm. 549, 306–316. https://doi.org/10.1016/j.ijpharm.2018.07.050.

Liao, X., Krishnamurthy, R., Suryanarayanan, R., 2007. Influence of processing conditions on the physical state of mannitol—implications in freeze-drying. Pharm. Res. 24, 370–376. https://doi.org/10.1007/s11095-006-9158-3.

Lu, D., Ma, Z., Zhang, T., Zhang, X., Wu, B., 2016. Metabolism of the anthelmintic drug niclosamide by cytochrome P450 enzymes and UDP-glucuronosyltransferases: metabolite elucidation and main contributions from CYP1A2 and UGT1A1. Xenobiotica 46, 1–13. https://doi.org/10.3109/00498254.2015.1047812.

Mahmood, I., 2014. Naive pooled-data approach for pharmacokinetic studies in pediatrics with a very small sample size. Am. J. Ther. 21, 269–274. https://doi.org/10.1097/MJT.0b013e31824ddee3.

Mattes, G., n.d. Enhancing Drug Delivery with Thin-Film Freezing Technology [WWW Document]. URL https://www.pharmasalmanac.com/articles/enhancing-drug-delivery-with-thin-film-freezing-technology (accessed 10.10.20).

Mehta, M., Bhardwaj, S.P., Suryanarayanan, R., 2013. Controlling the physical form of mannitol in freeze-dried systems. Eur. J. Pharm. Biopharm., SI: EJPB Freeze Drying (Invited only) 85, 207–213. https://doi.org/10.1016/j.ejpb.2013.04.010.

Mentré, F., Burtin, P., Merlé, Y., van Bree, J., Mallet, A., Steimer, J.-L., 1995. Sparse-sampling optimal designs in pharmacokinetics and toxicokinetics. Drug Inf. J. 29, 997–1019. https://doi.org/10.1177/009286159502900321.

Miller, K., McGrath, M.E., Hu, Z., Ariannejad, S., Weston, S., Frieman, M., Jackson, W.T., 2020. Coronavirus interactions with the cellular autophagy machinery. Autophagy 1–9. https://doi.org/10.1080/15548627.2020.1817280.

Molina, R.M., Konduru, N.V., Hirano, H., Donaghey, T.C., Adamo, B., Laurenzi, B., Pyrgiotakis, G., Brain, J.D., 2016. Pulmonary distribution of nanoceria: comparison of intratracheal, microspray instillation and dry powder insufflation. Inhal. Toxicol. 28, 550–560. https://doi.org/10.1080/08958378.2016.1226449.

Mönckedieck, M., Kamplade, J., Fakner, P., Urbanetz, N.A., Walzel, P., Steckel, H., Scherließ, R., 2017. Dry powder inhaler performance of spray dried mannitol with tailored surface morphologies as carrier and salbutamol sulphate. Int. J. Pharm. 524, 351–363. https://doi.org/10.1016/j.ijpharm.2017.03.055.

Mook, R.A., Wang, J., Ren, X.-R., Chen, M., Spasojevic, I., Barak, L.S., Lyerly, H.K., Chen, W., 2015. Structure-activity studies of Wnt/β-catenin inhibition in the Niclosamide chemotype: Identification of derivatives with improved drug exposure. Bioorg. Med. Chem. 23, 5829–5838. https://doi.org/10.1016/j.bmc.2015.07.001.

Moon, C., Sahakijpijarn, S., Koleng, J.J., Williams, R.O., 2019. Processing design space is critical for voriconazole nanoaggregates for dry powder inhalation produced by thin film freezing. J. Drug Deliv. Sci. Technol. 54, 101295. https://doi.org/10.1016/j.jddst.2019.101295.

Newman, J.A., Schmitt, P.D., Toth, S.J., Deng, F., Zhang, S., Simpson, G.J., 2015. Parts per Million Powder X-ray Diffraction. Anal. Chem. 87, 10950–10955. https://doi.org/10.1021/acs.analchem.5b02758.

Ohno, S., Nakajin, S., 2009. Determination of mRNA expression of human UDP-glucuronosyltransferases and application for localization in various human tissues by real-time reverse transcriptase-polymerase chain reaction. Drug Metab. Dispos. 37, 32–40. https://doi.org/10.1124/dmd.108.023598.

Patel, V., Sharma, O.P., Mehta, T.A., 2019. Impact of process parameters on particle size involved in media milling technique used for preparing clotrimazole nanocrystals for the management of cutaneous candidiasis. AAPS PharmSciTech 20, 175. https://doi.org/10.1208/s12249-019-1368-1.

Peters, B.-H., Staels, L., Rantanen, J., Molnár, F., De Beer, T., Lehto, V.-P., Ketolainen, J., 2016. Effects of cooling rate in microscale and pilot scale freeze-drying – variations in excipient polymorphs and protein secondary structure. Eur. J. Pharm. Sci., The 6th BBBB Conference on Pharmaceutical Sciences 95, 72–81. https://doi.org/10.1016/j.ejps.2016.05.020.

Pindiprolu, S.K.S.S., Pindiprolu, S.H., 2020. Plausible mechanisms of Niclosamide as an antiviral agent against COVID-19. Med. Hypotheses 140, 109765. https://doi.org/10.1016/j.mehy.2020.109765.

Ray, E., Vaghasiya, K., Sharma, A., Shukla, R., Khan, R., Kumar, A., Verma, R.K., 2020. Autophagy-inducing inhalable co-crystal formulation of niclosamide-nicotinamide for lung cancer therapy. AAPS PharmSciTech 21, 260. https://doi.org/10.1208/s12249-020-01803-z.

Romani, D., Noureddine, O., Issaoui, N., Brandán, S.A., 2020. Properties and reactivities of niclosamide in different media, a potential antiviral to treatment of COVID-19 by using DFT calculations and molecular docking. Biointerface Res. Appl. Chem. 7295–7328.

Sagan, P., n.d. TFF Pharmaceuticals Announces Topline Results of Voriconazole Inhalation Powder Phase 1 Clinical Trial [WWW Document]. BioSpace. URL https://www.biospace.com/article/tff-pharmaceuticals-announces-topline-results-of-voriconazole-inhalation-powder-phase-1-clinical-trial/ (accessed 1.15.21).

Sahakijpijarn, S., Smyth, H.D.C., Miller, D.P., Weers, J.G., 2020. Post-inhalation cough with therapeutic aerosols: formulation considerations. Adv. Drug Deliv. Rev. 165–166, 127–141. https://doi.org/10.1016/j.addr.2020.05.003.

Schweizer, M.T., Haugk, K., McKiernan, J.S., Gulati, R., Cheng, H.H., Maes, J.L., Dumpit, R.F., Nelson, P.S., Montgomery, B., McCune, J.S., Plymate, S.R., Yu, E.Y., 2018. A phase I study of niclosamide in combination with enzalutamide in men with castration-resistant prostate cancer. PLoS ONE 13. https://doi.org/10.1371/journal.pone.0198389.

Tonnis, W.F., Bagerman, M., Weij, M., Sjollema, J., Frijlink, H.W., Hinrichs, W.L.J., de Boer, A.H., 2014. A novel aerosol generator for homogenous distribution of powder over the lungs after pulmonary administration to small laboratory animals. Eur. J. Pharm. Biopharm. 88, 1056–1063. https://doi.org/10.1016/j.ejpb.2014.10.011.

Wu, C.-J., Jan, J.-T., Chen, C.-M., Hsieh, H.-P., Hwang, D.-R., Liu, H.-W., Liu, C.-Y., Huang, H.-W., Chen, S.-C., Hong, C.-F., Lin, R.-K., Chao, Y.-S., Hsu, J.T.A., 2004. Inhibition of severe acute respiratory syndrome coronavirus replication by niclosamide. Antimicrob. Agents Chemother. 48, 2693–2696. https://doi.org/10.1128/AAC.48.7.2693-2696.2004.

Wu, F., Zhao, S., Yu, B., Chen, Y.-M., Wang, W., Song, Z.-G., Hu, Y., Tao, Z.-W., Tian, J.-H., Pei, Y.-Y., Yuan, M.-L., Zhang, Y.-L., Dai, F.-H., Liu, Y., Wang, Q.-M., Zheng, J.-J., Xu, L., Holmes, E.C., Zhang, Y.-Z., 2020. A new coronavirus associated with human respiratory disease in China. Nature 579, 265–269. https://doi.org/10.1038/s41586-020-2008-3.

Xu, J., Shi, P.-Y., Li, H., Zhou, J., 2020. Broad Spectrum Antiviral Agent Niclosamide and Its Therapeutic Potential. ACS Infect. Dis. https://doi.org/10.1021/acsinfecdis.0c00052.

Xue, G., Gan, X., Wu, Z., Xie, D., Xiong, Y., Hua, L., Zhou, B., Zhou, N., Xiang, J., Li, J., 2020. Novel serological biomarkers for inflammation in predicting disease severity in patients with COVID-19. Int. Immunopharmacol. 107065 https://doi.org/10.1016/j.intimp.2020.107065.

Ye, Y., Zhang, X., Zhang, T., Wang, H., Wu, B., 2015. Design and evaluation of injectable niclosamide nanocrystals prepared by wet media milling technique. Drug Dev. Ind. Pharm. 41, 1416–1424. https://doi.org/10.3109/03639045.2014.954585.

Yj, K., S, S., Yj, C., 2021. Biological roles of cytochrome P450 1A1, 1A2, and 1B1 enzymes. Arch. Pharm. Res. 44, 63–83. https://doi.org/10.1007/s12272-021-01306-w.